Advanced Structural Mechanics 1 (2022) 1-13

Advanced Structural Mechanics

journal homepage: http://asm.sku.ac.ir

On the temperature-dependent nonlinear vibrations of functionally graded Timoshenko beams

Arash Davoudvand[a], Hadi Arvin[a,b,*], Krzystof Kamil Żur[c]

[a]*Faculty of Engineering, Shahrekord University, Shahrekord, Iran*
[b]*Nanotechnology Research Institute, Shahrekord University, Shahrekord, Iran*
[c]*Faculty of Mechanical Engineering, Bialystok University of Technology, Bialystok, Poland*

Article received:2022/08/30, Article revised: 2023/01/06, Article accepted: 2023/01/06

ABSTRACT

In this study, the nonlinear free vibrations of an elastically supported beam composed of functionally graded materials (FGMs) are investigated. The beam is in contact with a two-parameter elastic medium and is under a thermal environment. The thermomechanical properties of the beam are dependent on the temperature. Kinetic and strain energy relations for the FGM beam are obtained according to the Timoshenko beam theory and the von Karman nonlinear displacement strain relations. In order to obtain the ratio of nonlinear to linear natural frequencies, the Ritz method is used in cooperation with a direct repetition method. The results are represented in terms of boundary condition length-to-thickness ratio, volume fraction power of the constituents, temperature and elastic foundation parameters. The results show that the increased length-to-thickness ratio for FGM beams with S-S, C-S and C-C supports, decreases the ratio of the first nonlinear to linear natural frequency, while for an FGM beam with C-F support, the mentioned frequency ratio increases. Moreover, increasing the volume fraction power of the constituents for the FGM beam with S-S, C-S and C-C boundary conditions increases the aforesaid frequency ratio initially, and thereafter it decreases. Meanwhile, changing the mentioned power has no effect on the frequency ratio related to a C-F FGM beam.
Keywords: Nonlinear natural frequency; FGM beams; Elastic foundation; Large amplitude vibrations

1. Introduction

In modern machinery, a high operating speed is merged with lighter elements. This combination is one of the major reasons why nonlinear vibrations occur frequently in rotating machinery. Accordingly, the large amplitude vibration is a phenomenon that must be considered for structural design problems [1].

* Corresponding author at: Faculty of Engineering, Shahrekord University, Shahrekord, Iran.
E-mail address: hadi.arvin@sku.ac.ir.
DOI: 10.22034/asm.2023.14005.1005: http://asm.sku.ac.ir/article_11371.html

The FGM term was first proposed by a group of Japanese scientists in 1984 for materials that can be used as a barrier to prevent heat issues. An FGM is a combination created of at least two constituents usually a mixture of a ceramic and a metal. The ceramic phase improves the heat resistance to high temperatures thanks to its low thermal conductivity, meanwhile, the metal phase prevents breakage in high temperatures. FGMs are usually implemented in high-temperature environments. Furthermore, nowadays they have many applications in various industries such as aerospace, aircraft, and automobile manufacturing, nuclear reactors, and defense and electronics industries [2].

Mahmoudpour et al. [3] investigated the nonlinear vibrations of an FGM Euler-Bernoulli nanobeam employing a new stress-driven non-local integration technique. In their research, nonlinear natural frequencies evaluated according to the developed model were compared with their associated values obtained by Eringen's model. Loghman et al. [4] investigated the nonlinear vibrations of an FGM viscoelastic Euler-Bernoulli microbeam employing the modified couple stress theory (MCST). The presented results illustrated that increasing the fractional order of the viscoelastic microbeam increases the damping of the system. Hosseini and Arvin [5] used the MCST in order to obtain the fundamental pre-post buckling natural frequency of a rotating sandwich FGM Euler-Bernoulli microbeam. The finite element method (FEM) was used to discretize the governing equations. Thereafter, the Newton-Raphson method beside an iterative developed algorithm delivered the fundamental pre/post-buckling natural frequency. Davoudvand and Arvin [6] analyzed the first flapping backbone curve of a graphene-reinforced microbeam (a GPLRC microbeam) with various boundary condition types. The examined microbeam was modelled in the framework of the assumptions of Reddy's beam theory alongside the MCST. The results of their research showed that an S-S, a C-C and a C-F microbeam exhibit, sequently, the hardening, hardening and softening behaviours. Wang and Li [7] examined the natural frequencies of an FGM beam based on the Levinson beam hypothesis. They applied the shooting method for free vibration examination. Chen et al. [8] analyzed the free vibrations of an FGM beam employing a higher-order shear deformation theory with presenting an innovative transverse shear stress function. Keshmiri et al. [9] implemented the Adomian technique with the aim of examining the free vibration features of an FGM conical beam. Zhang et al. [10] investigated the natural frequencies of a clamped-clamed (C-C) and a clamped-free (C-F) FGM nanobeam resorting to the developed Wittrick-Williams algorithm. They declared that the increase of the non-local parameter likewise the power law exponent, sequentially, leads to a reduction and an enlargement in the associated natural frequencies. Tian et al. [11] established a semi-analytical model for free vibration examination of a rotating porous FGM beam. Arani and Soleimani [12] analyzed the small-scale natural frequencies and the corresponding loss factors of a sandwich beam with a magnetic fluid core and FGM face sheets exposed to a supersonic air flow. Malikan and Eremeyev [13] established an innovative hyperbolic-polynomial shear stress theory for the sake of investigating the defect effect on the corresponding critical buckling point. Zhu et al. [14] evaluated the dynamic treatment of a cracked FGM beam subjected to harmonic point loads. Li et al. [15] examined the natural frequencies of an FGM beam with non-uniform thickness submerged in the fluid. The large amplitude free vibration study of a damped and an undamped FGM beam was accomplished by Mohammadian [16]. An inclusive analysis on pre/post-buckling free vibrations of a rotating FGM Euler-Bernoulli beam was addressed by Arvin et al. [17] by applying the FEM. Sharma and Singh [18] established a numerical study on the free vibrations of an FGM Timoshenko beam by the implementation of the generalized quadratic differential method. Kouami et al. [19] utilized the FEM with the aim of the examination of the free vibrations of a sandwich viscoelastic FGM beam on the basis of the zigzag theory. Davoudvand et al. [20] addressed the fundamental amplitude-dependent transversal natural frequency of a GPLRC beam on an elastic foundation subjected to a uniform temperature increase in the framework of a high-order beam theory. The equations of motion were discretized by the Ritz-Chebyshev technique. The hardening or softening type of nonlinearity of the beam was discussed in detail for different boundary conditions types.

In this article, the large amplitude free vibrations of an FGM beam resting on an elastic foundation are addressed. The governing equations are achieved by implementing the Timoshenko beam theory alongside the von-Karman strains. By the implementation of the Chebyshev-Ritz method, the nonlinear stiffness matrix beside the mass matrix is achieved. An iterative scheme is established in order to determine the fundamental nonlinear natural frequency. A detailed discussion on the effects of the FGM characteristics as well as the boundary condition type on the linear natural frequencies likewise the fundamental nonlinear natural frequency is provided.

2. Geometric model and properties of FGM beams

A rectangular FGM beam with length L and thickness h resting on a Winkler-Pasternak elastic foundation is shown in Fig. 1. An inertial frame with the Cartesian coordinate system is situated at the left end of the mid-plane. The volume fractions of the ceramic and metal constituents are specified, sequently, by V_c and V_m. They are, respectively, denoted, as follows [21]:

$$V_{c1} = (1 + \frac{2z}{h})^k, -\frac{h}{2} \leq z \leq 0 \tag{1}$$

$$V_{c2} = (1 - \frac{2z}{h})^k, 0 < z \leq \frac{h}{2} \tag{2}$$

$$V_c = V_{c1} + V_{c2} \tag{3}$$

$$V_m = 1 - V_c \tag{4}$$

In Eqs. (1) and (2), k stands for the power law exponent that determines the contribution of the constituents in the FGM. Based on the common widget method every thermo-mechanical property of an FGM beam such as P can be expressed as follows [21]:

$$P(z,T) = (P_c(T) - P_m(T))\left(\frac{1}{2} + \frac{z}{h}\right)^k + P_m(T) \tag{5}$$

In Eq. (3), T represents the absolute temperature in K. P_c and P_m, respectively, express the associated properties of the ceramic and metal components used in the FGM beam. Feasible thermo-mechanical properties of the FGM such as Young modulus, mass density, and thermal expansion coefficient are quantified according to Eq. (5) meanwhile, a constant value for the Poisson's ratio is assumed.

3. Theoretical formulation and deriving the governing equations

Timoshenko beam theory is employed to obtain the strain and kinetic energies of the FGM beam. The associated longitudinal (U) and transversal (W) elements of the displacement field read [22]:

$$U(x,z,t) = u(x,t) + z\Psi(x,t) \tag{6}$$

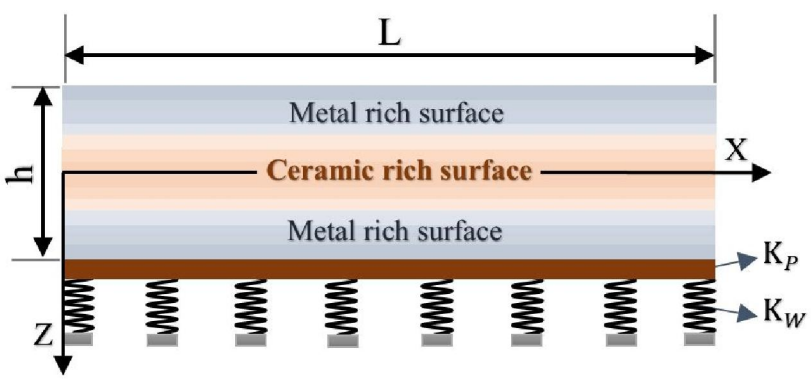

Fig. 1. FGM beam resting on a Winkler-Pasternak elastic foundation.

$$W(x,z,t) = w(x,t) \tag{7}$$

In Eqs. (6) and (7), u and w represent the longitudinal and transversal displacements toward the x and z directions, respectively, and Ψ denotes the bending rotation of the cross section of the beam at x. Considering the assumed displacement field, the normal (ε_{xx}) and shear (γ_{xz}) strains are defined, sequently, as follow [22, 23]:

$$\varepsilon_{xx} = \frac{\partial U}{\partial x} + \frac{1}{2}\left(\frac{\partial W}{\partial x}\right)^2 = \frac{\partial u(x,t)}{\partial x} + z\frac{\partial \Psi(x,t)}{\partial x} + \frac{1}{2}\left(\frac{\partial w(x,t)}{\partial x}\right)^2 \tag{8}$$

$$\gamma_{xz} = \frac{\partial U}{\partial z} + \frac{\partial W}{\partial x} = \frac{\partial w(x,t)}{\partial x} + \Psi(x,t) \tag{9}$$

According to Eqs. (8) and (9), the normal (σ_{xx}) and shear (τ_{xz}) stresses of the FGM beam exposed to a uniform temperature rising (ΔT) with respect to the normal and shear strains are obtained as follow [22, 23]:

$$\sigma_{xx} = E(z,T)(\varepsilon_{xx} - \alpha(z,T)\Delta T) \tag{10}$$

$$\tau_{xz} = K_s \frac{E(z,T)}{2(1+v)}\gamma_{xz} \tag{11}$$

where E represents the Young modulus of the FGM, α stands for its thermal expansion constant, and v denotes its Poisson's ratio. K_s is called the shear correction coefficient that is related to the geometry, and boundary conditions. Its numerical value for a rectangular beam is usually considered as $K_s = 5/6$ [19].

By applying Eqs. (8)-(11) and introducing the Winkler and Pasternak foundation effects, the virtual strain energy equation holds as [22]:

$$\delta U = \int_V (\sigma_{xx}\delta\varepsilon_{xx} + \tau_{xz}\delta\gamma_{xz})\,dV + \int_L \left(K_W W\delta W + K_P\frac{\partial w}{\partial x}\delta\frac{\partial w}{\partial x}\right)dx = \int_L \left(N_{xx}\left(\delta\frac{\partial u}{\partial x} + \left(\frac{\partial w}{\partial x}\delta\frac{\partial w}{\partial x}\right)\right) + M_{xx}\left(\delta\frac{\partial \Psi}{\partial x}\right) + Q_{xz}\left(\delta\frac{\partial w}{\partial x} + \delta\Psi\right) + K_W W\delta W + K_P\frac{\partial w}{\partial x}\delta\frac{\partial w}{\partial x}\right)dx \tag{12}$$

where the stress resultants are defined as follow:

$$N_{xx} = \int_A \sigma_{xx}dA = A_{11}\left(\frac{\partial u}{\partial x} + \frac{1}{2}\left(\frac{\partial w}{\partial x}\right)^2\right) + B_{11}\frac{\partial \Psi}{\partial x} - N_{th} \tag{13}$$

$$Q_{xz} = \int_A \tau_{xz}dA = A_{55}\left(\frac{\partial w}{\partial x} + \Psi\right) \tag{14}$$

$$M_{xx} = \int_A z\sigma_{xx}dA = B_{11}\left(\frac{\partial u}{\partial x} + \frac{1}{2}\left(\frac{\partial w}{\partial x}\right)^2\right) + D_{11}\frac{\partial \Psi}{\partial x} - M_{th} \tag{15}$$

By substituting Eqs. (13)-(15) into Eq. (12), the virtual strain energy is achieved in terms of the displacement field elements:

$$\delta U = \int \left(\left(A_{11}\left(\frac{\partial u}{\partial x} + \frac{1}{2}\left(\frac{\partial w}{\partial x}\right)^2\right) + B_{11}\frac{\partial \Psi}{\partial x} - N_{th}\right)\left(\delta\frac{\partial u}{\partial x} + \left(\frac{\partial w}{\partial x}\delta\frac{\partial w}{\partial x}\right)\right) + \left(B_{11}\left(\frac{\partial u}{\partial x} + \frac{1}{2}\left(\frac{\partial w}{\partial x}\right)^2\right) +$$

$$D_{11}\frac{\partial\Psi}{\partial x}-M_{th}\Big)\Big(\delta\frac{\partial\Psi}{\partial x}\Big)+\Big(A_{55}\Big(\frac{\partial w}{\partial x}+\Psi\Big)\Big)\Big(\delta\frac{\partial w}{\partial x}+\delta\Psi\Big)+(K_w w\delta w+K_p\frac{\partial w}{\partial x}\delta\frac{\partial w}{\partial x})\Big)dx \tag{16}$$

where A_{11}, B_{11} and D_{11}, respectively, represent the tensile stiffness, coupled tensile-bending stiffness, and bending stiffness. A_{55} stands for the shear stiffness. N_{th} and M_{th}, respectively, denote the thermal force and moment resultants. The introduced parameters are defined by:

$$(A_{11},B_{11},D_{11})=\int_A E(z)(1,z,z^2)dA \tag{17}$$

$$(N_{th},M_{th})=\int_A E(z)\alpha\Delta T(1,z)dA \tag{18}$$

$$(A_{55})=\int_A \frac{E(z)}{2(1+\nu)}dA \tag{19}$$

Considering the assumed displacement field for the FGM beam, the virtual kinetic energy can be expressed as follows [20]:

$$\begin{aligned}\delta T&=\int_V \rho(\frac{\partial U}{\partial t}\delta\frac{\partial U}{\partial t}+\frac{\partial W}{\partial t}\delta\frac{\partial W}{\partial t})dV\\&=\int_0^L\int_A \rho\left(\left(\frac{\partial u}{\partial t}+z\frac{\partial\Psi}{\partial t}\right)\delta\left(\frac{\partial u}{\partial t}+z\frac{\partial\Psi}{\partial t}\right)+\frac{\partial w}{\partial t}\delta\frac{\partial w}{\partial t}\right)dA\,dx\end{aligned} \tag{20}$$

Subsequently, the virtual kinetic energy of the FGM beam is reshuffled into:

$$\delta T=\int_0^L\left\{I_0\left(\frac{\partial u}{\partial t}\delta\frac{\partial u}{\partial t}+\frac{\partial w}{\partial t}\delta\frac{\partial w}{\partial t}\right)+I_1\left(\frac{\partial u}{\partial t}\delta\frac{\partial\Psi}{\partial t}+\frac{\partial\Psi}{\partial t}\delta\frac{\partial u}{\partial t}\right)+I_2\left(\frac{\partial\Psi}{\partial t}\delta\frac{\partial\Psi}{\partial t}\right)\right\}dx \tag{21}$$

where

$$(I_0,I_1,I_2)=\int\rho(z)(1,z,z^2)dA \tag{22}$$

Employing Eqs. (16) and (21) in Hamilton's principle, i.e. Eq. (23), the weak form of the governing nonlinear equations is achieved [24].

$$\delta\int_{t_1}^{t_2}(U-T)\,dt=0 \tag{23}$$

4. Dealing with the governing equations

Thanks to the advantages of Chebyshev-Ritz method including its applicability for a variety of boundary condition types this technique is implemented for the discretization of the nonlinear governing equations in space domain. Another advantage of this method is its direct application for discretizing the weak form of the governing equations. Subsequently, just the geometrical boundary condition types need to be justified by the assumed shape functions. This method considers the expansion of displacement elements in terms of unknown time dependent coefficients (A_i, B_i, C_i) multiplied by the predefined shape functions in the form of an infinite series. However, usually, assuming a sufficient number of series terms leads to a very high accurate solution in various fields of mechanics. In this regard, the shape functions are considered in terms of the Chebyshev polynomials ($T_i(x)$) multiplied by another functions

$(Rw(x), R\Psi(x), Ru(x))$ that satisfy the essential boundary conditions. Henceforth, the latter is called the essential functions. Subsequently, the displacement elements are regarded as follow [25, 26]:

$$w(x,t) = \sum_{i=1}^{n} A_i(t)\, Rw(x) T_i(x) \tag{24}$$

$$\Psi(x,t) = \sum_{i=1}^{n} B_i(t)\, R\Psi(x) T_i(x) \tag{25}$$

$$u(x,t) = \sum_{i=1}^{n} C_i(t)\, Ru(x) T_i(x) \tag{26}$$

where n represents the number of shape functions that lead to a proper convergence in a requested result. The Chebyshev polynomial elements ($T_i(x)$) for the FGM beam space domain ($[0\ L]$) are expressed in the form of the following recursive relation [27]:

$$T_1(x) = 1 \tag{27}$$

$$T_2(x) = \frac{2x}{L} - 1 \tag{28}$$

$$T_i(x) = 2\left(\frac{2x}{L} - 1\right)\left(T_{i-1}(x) - T_{i-2}(x)\right), i = 3 \text{ to } n \tag{29}$$

On the other hand, the essential functions for various boundary conditions are introduced in the polynomial style in Table 1.

By substituting Eqs. (24)-(26) into Eq. (23) and minimizing the ensuing relation based on the Ritz technique process, the nonlinear discretized governing equations for the FGM beam is achieved [28]:

$$M\ddot{X} + K_L X + K_{NL} X = 0 \tag{30}$$

where K_L, K_{NL} and M stand for the linear stiffness matrix, the nonlinear stiffness matrix and the mass matrix, respectively. The elements of the associated matrices are released in **Appendix A**. Also, $\mathrm{X} = [\mathrm{A}, \mathrm{B}, \mathrm{C}]^{\mathrm{T}}$ represents the generalized coordinate vector where $\mathrm{A} = \{A_1, A_2, \dots, A_n\}$, $\mathrm{B} = \{B_1, B_2, \dots, B_n\}$ and $\mathrm{C} = \{C_1, C_2, \dots, C_n\}$.

The following iterative algorithm reveals the amplitude dependent fundamental nonlinear natural frequency of the FGM beam. For different boundary conditions a sample point is chosen. The sample point for a C-F FGM beam is at the free end while for the other FGM beams with boundary conditions indicated in Table 1 the point at the mid-span is selected.

- At first, resorting to the linear stiffness matrix and the mass matrix, the eigenvalues and the mutual eigenvectors are calculated. They, sequently, deliver the linear natural frequencies and the associated linear modes
- The first eigenvector is scaled in such a way that it creates a deflection at the sample point of the FGM beam identical to the desired deflection at which the nonlinear natural frequency is requested. Accordingly, the nonlinear stiffness matrix is calculated.
- After calculating the nonlinear stiffness matrix, with the aid of Eq. (30) the associated eigenvalues and eigenvectors are calculated. The smallest calculated eigenvalue represents the first nonlinear natural frequency. By comparing

Table 1. Polynomial essential functions associated to various boundary conditions [25, 26].

Essential function	S-S FGM beam	C-C FGM beam	C-S FGM beam	C-F FGM beam
$Rw(x)$	$\left(\frac{x}{L}\right)\left(1-\frac{x}{L}\right)$	$\left(\frac{x}{L}\right)\left(1-\frac{x}{L}\right)$	$\left(\frac{x}{L}\right)\left(1-\frac{x}{L}\right)$	$\left(\frac{x}{L}\right)\left(1-\frac{x}{L}\right)^0$
$R\Psi(x)$	$\left(\frac{x}{L}\right)^0\left(1-\frac{x}{L}\right)^0$	$\left(\frac{x}{L}\right)\left(1-\frac{x}{L}\right)$	$\left(\frac{x}{L}\right)\left(1-\frac{x}{L}\right)^0$	$\left(\frac{x}{L}\right)\left(1-\frac{x}{L}\right)^0$
$Ru(x)$	$\left(\frac{x}{L}\right)\left(1-\frac{x}{L}\right)$	$\left(\frac{x}{L}\right)\left(1-\frac{x}{L}\right)$	$\left(\frac{x}{L}\right)\left(1-\frac{x}{L}\right)$	$\left(\frac{x}{L}\right)\left(1-\frac{x}{L}\right)^0$

the difference of the most recent two first eigenvalues the accuracy of the first nonlinear natural frequency at the desired deflection is examined. If the accuracy is acceptable the requested nonlinear natural frequency at the desired deflection has been determined. Otherwise, with the most recent eigen-vector the solution procedure is resumed from the second step.

5. Results and discussions

In this section, numerical results for the large amplitude free vibrations of the FGM beam resting on a Winkler-Pasternak elastic foundation subjected to a uniform temperature change are presented and discussed. The constituents of the FGM beam are stainless steel (SUS304) for the metal phase and silicon nitride (Si_3N_4) as the ceramic phase. The thermo-mechanical properties of both constituents are temperature dependent determined by the Touloukian model [29]:

$$P = P_0(P_{-1}T^{-1} + 1 + P_1T + P_2T^2 + P_3T^3) \tag{31}$$

where P_0, P_{-1}, P_1 , P_2 and P_3 are presented for both constituents in Table 2 for various thermo-mechanical properties.

The Winkler and Pasternak coefficients of the elastic foundation are normalized, respectively, as follow:

$$k_W = \frac{K_W\pi^4 D_{11m}}{L^4} \tag{32}$$

$$k_P = \frac{K_P\pi^2 D_{11m}}{L^2} \tag{33}$$

where D_{11m} is calculated with a relation similar to D_{11} but for the metal constituent at temperature 300 K.

5.1. Comparison examination

In the first comparative examination the first natural frequency of a C-C FGM beam is investigated. The free vibration analysis of the C-C FGM beam has been studied in the framework of the Timoshenko beam model in Ref. [30] and based on the Euler-Bernoulli beam model in Ref. [17]. The thermo-mechanical properties of the FGM constituents are identical to Table 2 and the power law exponent is $k = 1$. The slenderness ratio of the FGM beam is $L/h = 25$. Figure 2 shows the variation of the dimensionless first natural frequency (λ_1) in terms of the temperature change. The first dimensionless natural frequency is defined by $\lambda_1 = \omega_1 h\sqrt{\frac{12\rho_c}{E_{cref}}}(L/h)^2$ where ω_1 stands for the first dimensional natural frequency of the C-C FGM beam. ρ_c and E_{cref} denote, respectively, the mass density and the modulus of elasticity of the ceramic phase at temperature 300 K. An acceptable conformity among the three results is detected.

Table 2. Thermo-mechanical properties of the constituents of the FGM beam.

Material	Property	P_0	P_{-1}	P_1	P_2	P_3
SUS304	E(Pa)	$201.04e9$	0	$3.079e-4$	$-6.534e-7$	0
	$\alpha(\mathrm{K}^{-1})$	$12.33e-6$	0	$8.086e-6$	0	0
	$\rho(\mathrm{kg/m}^3)$			8166		
	ν			0.28		
Si_3N_4	E(Pa)	$348.43e9$	0	$-3.07e-4$	$2.16e-7$	$-8.946e-11$
	$\alpha(\mathrm{K}^{-1})$	$5.8723e-6$	0	$9.095e-4$	0	0
	$\rho(\mathrm{kg/m}^3)$			2170		
	ν			0.28		

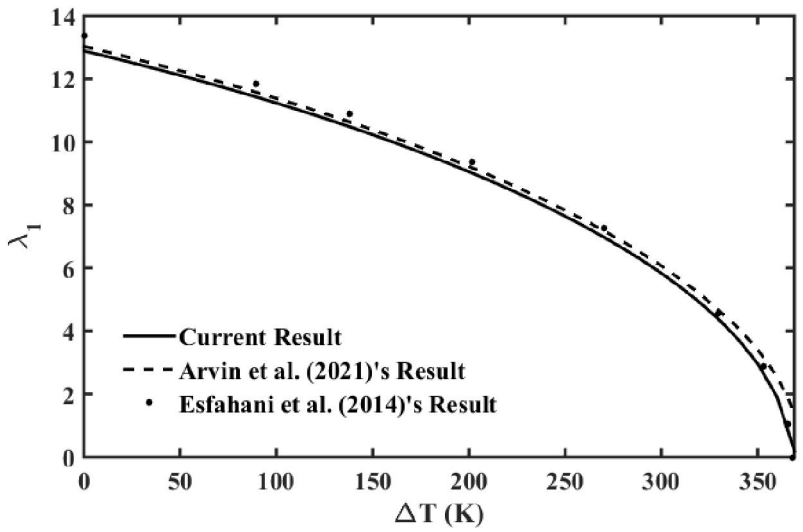

Fig. 2. The first dimensionless natural frequency of a C-C FGM beam in terms of the temperature.

In the second comparison study, the first nonlinear to linear natural frequency ratio for an isotropic Timoshenko beam with different boundary conditions has been examined. The results are compared with the associated results presented in Refs. [25] and [31] in Table 3. The length to thickness ratio of the isotropic Timoshenko beam is $L/h = 100$. The Young modulus, mass density and Poisson's ratio of the beam are 5 GPa, 1190 $\mathrm{Kg/m^3}$ and 0.3, respectively. The results have been presented for three different maximum vibration amplitudes divided by the radius of gyration ($\theta = \sqrt{\frac{I}{A}}$). Current results are in an accurate agreement with the associated results quantified in Refs. [25], and [31].

5.2. Parametric studies

After the endorsement of the proposed formulation and the solution methodology, several parametric studies are carried out in order to achieve the first nonlinear to linear natural frequency ratio in terms of the maximum deflection of an FGM beam resting on an elastic foundation exposed to a uniform temperature change. The thickness of the FGM beam is 0.01 m. Henceforth, the following information are assigned for numerical analyses unless new data is provided for some specific analyses. The slenderness ratio of the FGM beam is $L\ /\ h = 20$. The frequency ratio is quantified for the non-dimensional deflection of the sample point assigned as $\frac{w_{s-p}}{h} = 1$. The influence of the elastic foundation is ignored. The temperature is considered to be equal to the ambient temperature ($T = 300$ K). The power law exponent is specified as $k = 1$.

Table 4 shows the effect of the slenderness ratio on the first nonlinear to linear natural frequency ratio of the FGM beam considering the effect of boundary condition type. It can be seen that by increasing the slenderness ratio of the FGM beam with C-C and S-S boundary conditions, the first frequency ratio decreases. Meanwhile, at the same condition, for the C-S and C-F FGM beams the frequency ratio increases.
Furthermore, the largest and the smallest frequency ratio belong, sequently, to FGM beams with S-S and C-F supports.

Table 3. The first nonlinear to linear natural frequency ratio of an isotropic Timoshenko beam with different boundary conditions.

The slenderness ratio		S-S beam			C-C beam			C-S beam	
$w_{\max}/\theta$	Present	Ref. [25]	Ref. [31]	Present	Ref. [25]	Ref. [31]	Present	Ref. [25]	Ref. [31]
1	1.1193	1.1192	1.1181	1.0294	1.0303	1.0300	1.0580	1.0592	1.0595
2	1.4194	1.4180	1.4178	1.1159	1.1152	1.1147	1.2126	1.2179	1.2193
3	1.8150	1.8092	1.8094	1.2454	1.2419	1.2420	1.4452	1.4402	1.4448

Table 4. The effect of slenderness ratio on the first nonlinear to linear natural frequency ratio of an FGM beam with various boundary conditions.

The slenderness ratio	L/h=10	L/h=15	L/h=20	L/h=25	L/h=30	L/h=35	L/h=40
S-S	2.1039	2.0952	2.0921	2.0907	2.0900	2.0895	2.0892
C-S	1.7693	1.7728	1.7797	1.7872	1.7939	1.7990	1.8014
C-C	1.3498	1.3427	1.3406	1.3397	1.3392	1.3390	1.3388
C-F	0.9763	0.9987	0.9993	0.9995	0.9998	0.9998	0.9998

Table 5 exhibits the effect of the power law exponent on the first nonlinear to linear natural frequency ratio for an FGM beam with various boundary conditions. It can be seen that for the FGM beam with S-S, C-S and C-C supports, by means of increasing the power law exponent the frequency ratio increases initially and its maximum value is attained when $k = 2$. After the aforesaid value it starts to decrease. For a C-F FGM beam the frequency ratio is invariant with respect to the power law exponent.

Table 6 demonstrates the effect of the temperature rise on the first nonlinear to linear natural frequency ratio of an FGM beam with different boundary conditions and various power law exponents. It can be seen that for the FGM beam with S-S, C-S and C-C boundary conditions, the frequency ratio increases with the increase of the temperature. However, it can be seen that the frequency ratio of a C-F FGM beam is invariant with respect to the temperature change. Meanwhile, it is clear that the largest ratio of the frequency ratio belongs to an S-S FGM beam while the smallest has been determined for a C-F FGM beam.

Tables 7-10, respectively, present the effect of the elastic foundation parameters on the first nonlinear to linear natural frequency ratio of an FGM beam with S-S, C-S, C-C and C-F boundary conditions. The elastic foundation consists of two parameters, Winkler and Pasternak. Generally speaking, by means of increasing the values of the foundation parameters the frequency ratio decreases for every boundary conditions. From Table 7 it can be seen that for an S-S FGM beam the increase of the Winkler and Pasternak parameters to an identical value has the same influence in reducing the frequency ratio. Moreover, it can be comprehended from Tables 8-10 that for the FGM beam with the other boundary conditions, i.e. C-S, C-C and C-F FGM beams, the frequency ratio is less affected by increasing the Pasternak parameter rather than the Winkler parameter. Furthermore, the frequency ratio is invariant approximately with respect to the Winkler parameter for a C-F FGM beam. On the other hand, for the S-S, C-S and C-C FGM beams on an elastic foundation the maximum frequency ratio is determined for $k = 0$ although without taking into account the effect of elastic foundation the maximum frequency ratio belongs to $k = 2$. In addition, a very slight effect of the Pasternak parameter on the frequency ratio of a C-F FGM beam is observed.

Table 5. The effect of the power law exponent on the first nonlinear to linear natural frequency ratio of an FGM beam with various boundary conditions.

The power law exponent	$k = 0$	$k = 0.5$	$k = 1$	$k = 2$	$k = 3$	$k = 4$	$k = 5$
S-S	2.0036	2.0714	2.0921	2.0927	2.0822	2.0719	2.0634
C-S	1.7161	1.7648	1.7797	1.7801	1.7726	1.7625	1.7591
C-C	1.3089	1.3331	1.3406	1.3408	1.3370	1.3333	1.3302
C-F	0.9993	0.9993	0.9993	0.9993	0.9993	0.9993	0.9993

Table 6. The effect of the temperature rise on the first nonlinear to linear natural frequency ratio of an FGM beam with various boundary conditions and different power law exponents.

Support Condition	The power law exponent	$k = 0$	$k = 0.5$	$k = 1$	$k = 2$	$k = 3$	$k = 4$	$k = 5$
S-S	$\Delta T = 0$ K	2.0036	2.0714	2.0921	2.0927	2.0822	2.0719	2.0634
	$\Delta T = 50$ K	2.1721	2.3506	2.4330	2.4888	2.4985	2.4966	2.4920
	$\Delta T = 100$ K	2.4403	2.9251	3.2576	3.6301	3.8001	3.8835	3.9277
C-S	$\Delta T = 0$ K	1.7161	1.7648	1.7797	1.7801	1.7726	1.7625	1.7591
	$\Delta T = 50$ K	1.7937	1.8887	1.9281	1.9494	1.9492	1.9448	1.9399
	$\Delta T = 100$ K	1.8990	2.0799	2.1734	2.2484	2.2699	2.2753	2.2755
C-C	$\Delta T = 0$ K	1.3089	1.3331	1.3406	1.3408	1.3370	1.3333	1.3302
	$\Delta T = 50$ K	1.3229	1.3548	1.3662	1.3695	1.3668	1.3635	1.3606
	$\Delta T = 100$ K	1.3393	1.3816	1.3985	1.4066	1.4055	1.4028	1.4002
C-F	$\Delta T = 0$ K	0.9993	0.9993	0.9993	0.9993	0.9993	0.9993	0.9993
	$\Delta T = 50$ K	0.9993	0.9993	0.9993	0.9993	0.9993	0.9993	0.9993
	$\Delta T = 100$ K	0.9993	0.9993	0.9993	0.9993	0.9993	0.9993	0.9993

Table 7. The effect of elastic foundation parameters on the first nonlinear to linear natural frequency ratio of an FGM S-S beam.

The power law exponent	$k=0$	$k=0.5$	$k=1$	$k=2$	$k=3$	$k=4$	$k=5$
$k_P=0, k_W=0$	2.0036	2.0714	2.0921	2.0927	2.0822	2.0719	2.0634
$k_P=5, k_W=0$	1.2244	1.2060	1.1955	1.1841	1.1780	1.1742	1.1716
$k_P=0, k_W=5$	1.2244	1.2060	1.1955	1.1841	1.1780	1.1742	1.1717
$k_P=5, k_W=5$	1.1277	1.1153	1.1086	1.1016	1.0979	1.0957	1.0942
$k_P=10, k_W=0$	1.1277	1.1153	1.1086	1.1016	1.0979	1.0957	1.0942
$k_P=0, k_W=10$	1.1278	1.1153	1.1086	1.1016	1.0980	1.0958	1.0943
$k_P=10, k_W=10$	1.0686	1.0612	1.0574	1.0535	1.0515	1.0503	1.0495

Table 8. The effect of elastic foundation parameters on the first nonlinear to linear natural frequency ratio of an FGM C-S beam.

The power law exponent	$k=0$	$k=0.5$	$k=1$	$k=2$	$k=3$	$k=4$	$k=5$
$k_P=0, k_W=0$	1.7161	1.7648	1.7797	1.7801	1.7726	1.7625	1.7591
$k_P=5, k_W=0$	1.2032	1.1883	1.1794	1.1694	1.1639	1.1605	1.1582
$k_P=0, k_W=5$	1.2311	1.2155	1.2059	1.1950	1.1890	1.1852	1.1826
$k_P=5, k_W=5$	1.1251	1.1133	1.1955	1.1001	1.0966	1.0944	1.0930
$k_P=10, k_W=0$	1.1187	1.1078	1.1018	1.0954	1.0920	1.0900	1.0886
$k_P=0, k_W=10$	1.1389	1.1264	1.1196	1.1123	1.1085	1.1061	1.1046
$k_P=10, k_W=10$	1.0678	1.0606	1.0568	1.0529	1.0510	1.0498	1.0490

Table 9. The effect of elastic foundation parameters on the first nonlinear to linear natural frequency ratio of an FGM C-C beam.

The power law exponent	$k=0$	$k=0.5$	$k=1$	$k=2$	$k=3$	$k=4$	$k=5$
$k_P=0, k_W=0$	1.3089	1.3331	1.3406	1.3408	1.3370	1.3333	1.3302
$k_P=5, k_W=0$	1.1439	1.1387	1.1343	1.1284	1.1247	1.1223	1.1206
$k_P=0, k_W=5$	1.1642	1.1603	1.1561	1.1499	1.1459	1.1432	1.1413
$k_P=5, k_W=5$	1.1008	1.0943	1.0902	1.0852	1.0825	1.0807	1.0795
$k_P=10, k_W=0$	1.0939	1.0878	1.0839	1.0793	1.0767	1.0751	1.0740
$k_P=0, k_W=10$	1.1120	1.1058	1.1015	1.0963	1.0933	1.0914	1.0901
$k_P=10, k_W=10$	1.0597	1.0544	1.0515	1.0482	1.0465	1.0454	1.0447

Table 10. The effect of elastic foundation parameters on the first nonlinear to linear natural frequency ratio of an FGM C-F beam.

The power law exponent	$k=0$	$k=0.5$	$k=1$	$k=2$	$k=3$	$k=4$	$k=5$
$k_P=0, k_W=0$	0.9993	0.9993	0.9993	0.9993	0.9993	0.9993	0.9993
$k_P=5, k_W=0$	0.9991	0.9991	0.9990	0.9990	0.9990	0.9990	0.9990
$k_P=0, k_W=5$	0.9993	0.9993	0.9992	0.9992	0.9992	0.9992	0.9992
$k_P=5, k_W=5$	0.9990	0.9990	0.9990	0.9990	0.9990	0.9990	0.9990
$k_P=10, k_W=0$	0.9990	0.9990	0.9990	0.9990	0.9990	0.9990	0.9990
$k_P=0, k_W=10$	0.9992	0.9992	0.9992	0.9992	0.9992	0.9992	0.9992
$k_P=10, k_W=10$	0.9989	0.9989	0.9988	0.9988	0.9988	0.9988	0.9988

6. Conclusions

In this research the large amplitude free vibrations of an FGM beam resting on elastic foundation subjected to a uniform temperature rising was discussed. The Chebyshev-Ritz technique alongside an iterative algorithm delivered the fundamental nonlinear amplitude dependent natural frequency. The impacts of power law exponent, temperature change, elastic foundation parameters, and boundary conditions on the fundamental nonlinear to linear natural frequency ratio were examined. It was deduced that;

- The same amount of dimensionless Winkler and Pasternak constants has the same influence on the nonlinear frequency ratio of an S-S FGM beam.
- The maximum nonlinear frequency ratio for an FGM beam without considering the elastic foundation effect happens for the power law exponent equal to $k=2$, while regarding the elastic foundation effect the maximum takes pale for $k=0$.
- The nonlinear frequency ratio is invariant with respect to the Winkler effect.
- With the increase of the temperature the nonlinear frequency ratio enlarges.

Appendix A.

The mass matrix (M):

$$\mathrm{M} = \begin{bmatrix} M^{11} & 0 & 0 \\ 0 & M^{22} & M^{23} \\ 0 & M^{32} & M^{33} \end{bmatrix}$$

in which the elements of the mass matrix are specified as follow:

$$M^{11} = \int_0^L \left(I_0 Rw(x) T_i(x) Rw(x) T_j(x) \right) dx$$
$$M^{22} = \int_0^L \left(I_2 R\Psi(x) T_i(x) R\Psi(x) T_j(x) \right) dx$$
$$M^{23} = \int_0^L \left(I_1 Ru(x) T_i(x) R\Psi(x) T_j(x) \right) dx$$
$$M^{32} = \int_0^L \left(I_1 Ru(x) T_j(x) R\Psi(x) T_i(x) \right) dx$$
$$M^{33} = \int_0^L \left(I_0 Ru(x) T_i(x) Ru(x) T_j(x) \right) dx$$

The Linear stiffness matrix (K_L):

$$\mathrm{K}_L = \begin{bmatrix} K_L^{11} & K_L^{12} & 0 \\ K_L^{21} & K_L^{22} & K_L^{23} \\ 0 & K_L^{32} & K_L^{33} \end{bmatrix}$$

in which the elements of the linear stiffness matrix are defined as follow:

$$K_L^{11} = \int_0^L \Big((A_{55} - N_{th}) \frac{d}{dx} (Rw(x) T_i(x)) \frac{d}{dx} (Rw(x) T_j(x)) + K_w Rw(x)^2 T_i(x) T_j(x) + K_p \frac{d}{dx} (Rw(x) T_i(x)) \frac{d}{dx} (Rw(x) T_j(x)) \Big) dx$$
$$K_L^{12} = \int_0^L \left(A_{55} R\Psi(x) T_i(x) \frac{d}{dx} (Rw(x) T_j(x)) \right) dx$$
$$K_L^{21} = \int_0^L \left(A_{55} R\Psi(x) T_j(x) \frac{d}{dx} (Rw(x) T_i(x)) \right) dx$$
$$K_L^{22} = \int_0^L \left(D_{11} \frac{d}{dx} \left(R\Psi(x) T_i(x) \right) \frac{d}{dx} \left(R\Psi(x) T_j(x) \right) + A_{55} R\Psi(x) T_i(x) R\Psi(x) T_j(x) \right) dx$$
$$K_L^{23} = \int_0^L \left(B_{11} \frac{d}{dx} (Ru(x) T_i(x)) \frac{d}{dx} (R\Psi(x) T_j(x)) \right) dx$$
$$K_L^{32} = \int_0^L \left(B_{11} \frac{d}{dx} (Ru(x) T_j(x)) \frac{d}{dx} (R\Psi(x) T_i(x)) \right) dx$$
$$K_L^{33} = \int_0^L \left(A_{11} \frac{d}{dx} (Ru(x) T_i(x)) \frac{d}{dx} (Ru(x) T_j(x)) \right) dx$$

The nonlinear stiffness matrix (K_{NL}):

$$\mathrm{K}_{NL} = \begin{bmatrix} K_{NL}^{11} & K_{NL}^{12} & 0 \\ K_{NL}^{21} & 0 & 0 \\ K_{NL}^{31} & 0 & 0 \end{bmatrix}$$

in which the elements of the nonlinear stiffness matrix are determined as follow:

$$K_{NL}^{11} = \int_0^L \Big((A_{11} (\frac{du}{dx}) \frac{d}{dx} (Rw(x) T_i(x)) \frac{d}{dx} (Rw(x) T_j(x))) + 0.5 (A_{11} \left(\frac{dw}{dx} \right)^2 \frac{d}{dx} (Rw(x) T_i(x)) \frac{d}{dx} (Rw(x) T_j(x))) \Big) dx$$
$$K_{NL}^{12} = \int_0^L \left(B_{11} \left(\frac{dw}{dx} \right) \frac{d}{dx} \left(R\Psi(x) T_i(x) \right) \frac{d}{dx} \left(Rw(x) T_j(x) \right) \right) dx$$
$$K_{NL}^{21} = 0.5 \int_0^L \left(B_{11} \left(\frac{dw}{dx} \right) \frac{d}{dx} (R\Psi(x) T_j(x)) \frac{d}{dx} (Rw(x) T_i(x)) \right) dx$$

$$K_{NL}^{31} = 0.5 \int_0^L \left(A_{11} (\frac{dw}{dx}) \frac{d}{dx} (Ru(x) T_j(x)) \frac{d}{dx} (Rw(x) T_i(x)) \right) dx$$

References

[1] Jauregui, J.C., 2014. Parameter identification and monitoring of mechanical systems under nonlinear vibration. Woodhead Publishing, Cambridge.

[2] Pradhan, K.K., Chakraverty, S., 2013. Free vibration of Euler and Timoshenko functionally graded beams by Rayleigh–Ritz method, Composites Part B: Engineering. 51, 175-184.

[3] Mahmoudpour, E., Hashemi, SH.H., Faghidian, S.A., 2018. Nonlinear vibration analysis of FG nano-beams resting on elastic foundation in thermal environment using stress-driven nonlocal integral model. Applied Mathematical Modelling. 57, 302-315.

[4] Loghman, E., Kamali, A., Bakhtiari-Nejad, F., Abbaszadeh, M., 2021. Nonlinear free and forced Vibrations of fractional modeled viscoelastic FGM micro-beam. Applied Mathematical Modelling. 92, 297-314.

[5] Hosseini, S.M.H., Arvin, H., 2021. Free vibration analysis of pre/post-buckled rotating functionally graded sandwich micro-beams. Microsystem Technologies. 27, 2049-2061.

[6] Davoudvand, A., Arvin, H., 2023. Size dependent thermal backbone curves for nanocomposite Reddy micro-beams reinforced with grapheme platelets on elastic foundation. Mechanics of Composite Materials. *Accepted for publication*.

[7] Wang, X., Li, S., 2016. Free vibration analysis of functionally graded material beams based on Levinson beam theory. Applied Mathematics and Mechanics. 37(7), 861-878.

[8] Chen, Y., Jin, G., Zhang, C., Ye, T., Xue, Y., 2018. Thermal vibration of FGM beams with general boundary conditions using a higher order shear deformation theory. Composites Part B: Engineering. 153, 376-386.

[9] Keshmiri, A., Wu, N., Wang, Q., 2018. Vibration analysis of non-uniform tapered beams with nonlinear FGM properties. Journal of Mechanical Science and Technology. 32, 5325-5337.

[10] Zhang, K., Ge, M.H., Zhao, C., Deng, Z.C., Xu, X.J., 2019. Free vibration of nonlocal Timoshenko beams made of functionally graded materials by Symplectic method. Composites Part B: Engineering. 156, 174-184.

[11] Tian, J., Zhang, Z., Hua, H., 2019. Free vibration analysis of rotating functionally graded double-tapered beam including porosities. International Journal of Mechanical Sciences. 150, 526-538.

[12] Arani, A.G., Soleymani, T., 2019. Size-dependent vibration analysis of an axially moving sandwich beam with MR core and axially FGM faces layers in yawed supersonic airflow. European Journal of Mechanics-A/Solids. 77, 103792.

[13] Malikan, M., Eremeyev, V.A., 2020. A new hyperbolic-polynomial higher-order elasticity theory for mechanics of thick FGM beams with imperfection in the material composition. Composite Structures. 249, 112486.

[14] Zhu, L.F., Ke, L.L., Xiang, Y., Zhu ,X.Q., Wang, Y.,S. 2020. Vibrational power flow analysis of cracked functionally graded beams. Thin-Walled Structures. 150, 106626.

[15] Li, H.C., Ke, L.L., Yang, J., Kitipornchai, S., Wang, Y.S., 2020. Free vibration of variable thickness FGM beam submerged in fluid, Composite Structures. 228, 111582.

[16] Mohammadian, M., 2021. Nonlinear free vibration of damped and undamped bi-directional functionally graded beams using a cubic-quintic nonlinear model. Composite Structures. 225, 112866.

[17] Arvin, H., Hosseini, S.M.H., Kiani, Y., 2021. Free vibration analysis of pre/post buckled rotating functionally graded beams subjected to uniform temperature rise. Thin-Walled Structures. 158, 107187.

[18] Sharma, P., Singh, R., 2021. A numerical study on free vibration analysis of axial FGM beam. Materials Today: Proceedings. 44, 1664-1668.

[19] Kouami, K., Foudil, M., Mostafa, D.E., Erasmo, C., 2021. A finite element approach for the static and vibration analyses of functionally graded material viscoelastic sandwich beams with nonlinear material behavior. Composite Structures. 274, 114315.

[20] Davoudvand, A., Arvin, H., Kiani, Y., 2022. Thermal backbone curves of nanocomposite beams reinforced with graphene platelet on elastic foundation. International Journal of Structural Stability and Dynamics. 22(13), 2250147.

[21] Komijani, M., Esfahani, S.E., Reddy, J.N., Liu, Y.P., Eslami, M.R., 2014. Nonlinear thermal stability and vibration of pre/post-buckled temperature-and microstructure-dependent functionally graded beams resting on elastic foundation. Composite Structures. 112, 292-307.

[22] Reddy, J.N., 2003. Mechanics of laminated composite plates and shells: theory and analysis, second ed. CRC press, Boca Raton.

[23] Wang, C., Reddy, J.N., Lee, K., 2000. Shear deformable beams and plates: Relationships with classical solutions. Elsevier, Oxford.

[24] Meirovitch, L., 2000. Fundamentals of vibrations, McGraw Hill, New York.

[25] Ke, L.L., Yang, J., Kitipornchai, S., 2010. Nonlinear free vibration of functionally graded carbon nanotube-reinforced composite beams. Composite Structures. 92(3), 676-683.

[26] Mirzaei, M., Kiani, Y., 2016. Nonlinear free vibration of temperature-dependent sandwich beams with carbon nanotube-reinforced face sheets. Acta Mechanical. 227(7), 1869-1884.

[27] Abbaspour, F., Arvin H., 2021. Vibration analysis of piezoelectric graphene platelets micro-plates. AUT Journal of Mechanical Engineering. 5(3), 361-386.

[28] Reddy, J.N., 2014. An Introduction to Nonlinear Finite Element Analysis Second Edition: with applications to heat transfer, fluid mechanics, and solid mechanics. Second ed. Oxford University Press, Oxford.

[29] Reddy, J.N., Chin, C.D., 1998. Thermomechanical analysis of functionally graded cylinders and plates. Journal of Thermal Stresses. 21(6), 593–626.

[30] Esfahani, S.E., Kiani, Y., Komijani, M., Eslami, M.R., 2014. Vibration of a temperature-dependent thermally pre/postbuckled FGM beam over a nonlinear hardening elastic foundation. Journal of Applied Mechanics. 81(1), 011004.
[31] Marur, S.R., Prathap, G., 2005. Non-linear beam vibration problems and simplifications in finite element models. Computational Mechanics. 35, 352–360.